Adaptive optical two-photon microscopy using autofluorescent guide stars

Xiaodong Tao,* Andrew Norton, Matthew Kissel, Oscar Azucena, and Joel Kubby

Jack Baskin School of Engineering, University of California, Santa Cruz, 1156 High St., MS:SOE2 Santa Cruz, California 95064, USA
**Corresponding author: xiaod.tao@gmail.com*

Received July 29, 2013; revised October 19, 2013; accepted October 22, 2013;
posted October 23, 2013 (Doc. ID 194754); published November 25, 2013

We demonstrate a fast, direct wavefront-sensing method for dynamic *in vivo* adaptive optical two-photon microscopy. By using a Shack–Hartmann wavefront sensor and open-loop control, the system provides high-speed wavefront measurement and correction. To measure the wavefront in the middle of a Drosophila embryo at early stages, autofluorescence from endogenous fluorophores in the yolk were used as reference guide stars. The method was tested through live imaging of a Drosophila embryo. The aberration in the middle of the embryo was measured directly for the first time. After correction, the contrast and signal intensity of the structure in the middle of the embryo was improved. © 2013 Optical Society of America

OCIS codes: (110.1080) Active or adaptive optics; (010.7350) Wave-front sensing; (180.2520) Fluorescence microscopy; (180.6900) Three-dimensional microscopy; (170.3880) Medical and biological imaging.
http://dx.doi.org/10.1364/OL.38.005075

The ability to image intact tissues and living animals with high resolution and depth penetration makes two-photon microscopy an invaluable tool for studying the structure and function of cellular constituents within scattering tissue. Compared with the visible light used in confocal microscopy, the near-infrared beams used in two-photon microscopy experience less scattering from biological tissue. Furthermore, the light detection is more efficient where ballistic and diffused emission light is collected [1]. However, the penetration depth is still limited by scattering and optical aberration. The optical aberration is caused by the variation in refractive index from the inhomogeneous optical properties of the tissues and the refractive index mismatch between the tissue and mounting medium. To overcome this issue, adaptive optics has been successfully applied in microscopy [2]. Most of the adaptive optical (AO) microscopes developed so far are based on indirect methods of wavefront measurement, which utilize processing of the final image [3–6]. The extended exposure time causes photo bleaching and limits the bandwidth for live imaging. To increase the wavefront-correction speed, direct wavefront measurement is a promising method for dynamic *in vivo* imaging applications. In order to measure the wavefront error, wavefront sensors often require a guide star, which is a reference point source behind the inhomogeneous medium for measuring the shape of the wavefront. Injected microspheres and fluorescent proteins have been applied in wide-field and confocal microscopes as guide stars [7–9]. A nonlinear guide star using two-photon excitation has been demonstrated for correcting coupling and focusing aberrations in two-photon microscopy [10]; however, their long 800 ms integration time for making wavefront measurements is too slow for the dynamic *in vivo* imaging we require.

Here we demonstrate a fast (30 ms) direct wavefront measurement method in an AO two-photon microscope (AOTPM) using autofluorescent guide stars. As a label-free method, no special sample preparation is required. Autofluorescence from retinal lipofuscin by one-photon excitation has been used as a linear guide star to measure the wavefront of the human eye in vision science [11]. Here we demonstrate it in dynamic *in vivo* biological microscopy by combining it with two-photon excitation, where only the fluorophores at the focus plane are excited for generation of a guide star with minimal background noise. The intrinsic fluorophores are illuminated by a near-infrared ultrashort-pulsed laser with an appropriate wavelength, which is often different from the excitation wavelength of fluorescent proteins such as green fluorescent protein (GFP) and red fluorescent protein (RFP) [12]. This will induce less photo bleaching to the labeled fluorescent proteins during wavefront sensing. This method is particularly well suited when the fluorescence from fluorescent proteins is too weak for wavefront sensing. After wavefront measurement, the measured wavefront error was compensated by a deformable mirror (DM) using an open-loop control [13]. High-speed and high-performance wavefront measurement and correction are the critical advantages of direct wavefront measurement over other sensor-less AO systems. The proposed method was tested through live imaging of a Drosophila embryo labeled with GFP and RFP. This is the first time that aberrations have been measured in the middle of the Drosphila embryo.

The layout of the AOTPM is shown in Fig. 1. The system was designed and optimized using the optical-design software CODE V. The two-photon excitation is generated by a tunable (680–1080 nm) mode-locked Ti:Sapphire laser (140 fs, 80 MHz, Chameleon Ultra II, Coherent). The intensity of the laser is modulated by an electro-optic modulator (model 350-80LA, Conoptics Inc.). A 60× water-immersion objective with a numerical aperture of 1.2 was used (Olympus Microscope) for imaging. In order to correct the wavefront, a DM (Boston Micromachines) with 140 actuators and 3.5 μm of stroke is placed in the optical path, where it is conjugate to the exit pupil of the objective, the X and Y scanners, and the wavefront sensor. The optical system includes three telescope relay subsystems. Lenses L1 and L2 image the exit pupil of the objective lens onto the X scanner. They demagnify the pupil from 7.2 to 4 mm. Lenses L3 and L4 relay the X scanner conjugate to the Y scanner. This design minimizes the movement of the scanning

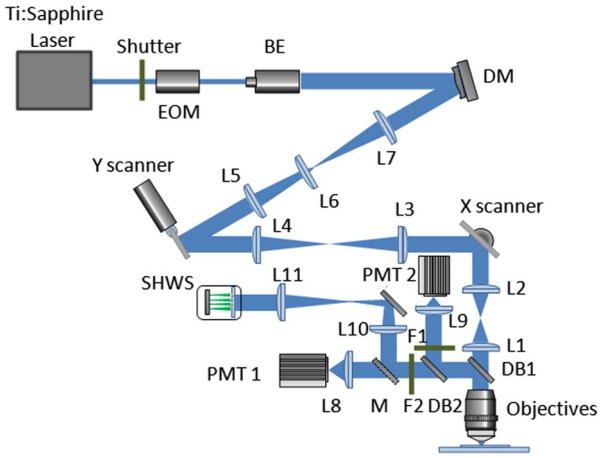

Fig. 1. Schematic of AO two-photon microscope: L, lens; F, filter; M, mirror flipper; BE, beam expender; EOM, electro-optic modulator; DM, deformable mirror; DB, dichroic beam splitters; SHWS, Shack–Hartmann wavefront sensor; PMT, photomultiplier tube. See text for details.

beam at the exit pupil of the objective lens and the emission light at the DM, which is important for accurate wavefront measurement and correction. Lenses L2 and L4 also serve as scanning lenses. The current design is optimized for an optical scanning angle of 4.4 degrees, which provides a field of view of 128 μm on the sample with a 60× objective. Lenses L5, L6, and L7 image the pupil of the Y scanner onto the DM. For nondescanned detection, two photomultiplier tubes (H7422-20 and H7421-40, Hamamatsu) and lenses L8 and L9 are located immediately after the objective lens, which collects the emitted light. The emission light is separated by single edge dichroic beam splitters (FF705-Di01, Semrock) for dual-color imaging. During wavefront measurement, two-photon images are captured first. A guide-star searching algorithm detects the best guide star based on the intensity and location from the image [14]. Then two galvo scanners (6215H, Cambridge Technology) steer the beam to the best location in the sample to generate a guide star. The Shack–Hartmann wavefront sensor (SHWS) with a 44×44 element lenslet array (AOA Inc.) and an electron multiplying CCD camera (Photometrics) utilizes the emission light from the sample for wavefront measurement. Because the SHWS and DM are located on the emission and excitation paths, respectively, open-loop DM control is applied. This configuration will eliminate additional dichroic mirrors and switchable mounts for a closed-loop configuration, where the SHWS should be located behind the DM.

To achieve open-loop control of the DM, an accurate model and calibration procedure are required. In our system, we apply mathematical modeling of the mirror surface based on the thin plate equation as follows [13]:

$$\nabla^4 \omega(r) = f_P(r)/D, \tag{1}$$

where $f_P(r)$ is the plate force, ω is the displacement of the plate, and D is the flexural rigidity of the plate. The plate force is the sum of spring forces $f_S(\omega)$ and electrostatic forces $f_E(\upsilon, \omega)$, where υ denotes voltage applied on the actuator. $f_S(\omega)$ and $f_E(\upsilon, \omega)$ can be calculated from displacement measurement during calibration. Accurate look-up tables of these two parameters for different υ and ω are generated [13]. During the system operation, the desired wavefront for compensation of the tissue-induced aberration is measured by the SHWS. Then the plate force $f_P(r)$ is calculated using Eq. (1), and $f_S(\omega)$ is retrieved from look-up tables based on the desired displacement ω of the mirror surface. Finally, the desired voltage υ on the DM is estimated from the look-up table, $f_E(\upsilon, \omega)$. A Zygo interferometer was used to measure surface displacement during the calibration. The root-mean-square (RMS) error of the open-loop control is around 17 nm for an amplitude of 500 nm.

To make an accurate wavefront measurement using the SHWS, the guide star should be smaller than the diffraction limit of the wavefront sensor. Also the number of photons coming from the guide star should be high enough to provide the required signal-to-noise ratio for the wavefront measurement. Thanks to the nonlinear excitation, the fluorescent emission is localized to a small, restricted area, which is often small enough to use as a guide star [10]. However, the intensity of the guide star highly depends on the distribution of the fluorescently labeled structure. An example shown in Fig. 2 is the two-photon image of a Drosophila embryo labeled with GFP and RFP excited by a laser with different wavelengths at a depth of 51 μm. The laser power at the sample is 17.5 mw. At 1000 nm excitation, most of the RFP labeled nuclei structure can be observed near the membrane. In the middle of the embryo, because the yolk induces large amounts of aberration and scattering, the intensity of the nuclei structure becomes much dimmer. At 920 nm excitation, GFP labeled centrosomes are also seen to be distributed near the membrane as shown in Fig. 2(b). It is extremely difficult to use this

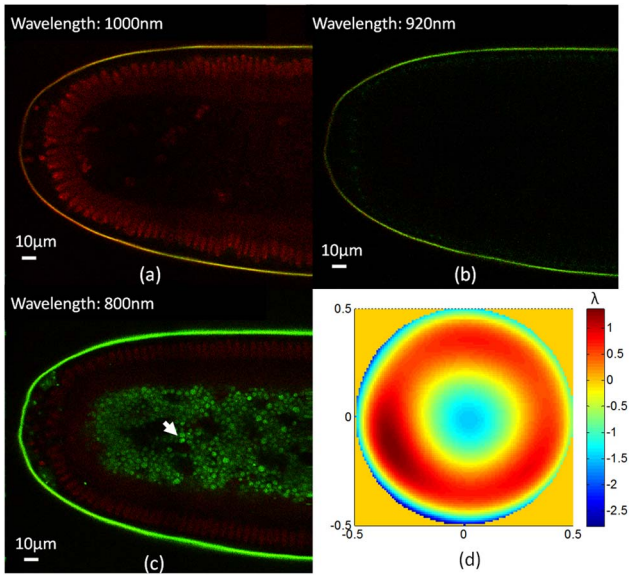

Fig. 2. Two-photon images of a Drosophila embryo at a depth of 51 μm with excitation wavelengths of (a) 1000 nm, (b) 920 nm, and (c) 800 nm. The wavefront (d) at the middle of embryo is measured by a SHWS in 30 ms using an autofluorescent guide star. During wavefront sensing, the laser illuminates the intrinsic fluorophores indicated by an arrow shown in (c). The scale bars are 10 μm.

fluorescence as a guide star in the middle of the embryo. Unfortunately, the mitosis process early in the development of the embryo (first nine cycles) occurs at the middle of the embryo, where the first cycles last for 10 min and begin once the egg has been laid [15]. High-resolution and high-speed imaging of this process are critical for this study. In the Drosophila embryo, a major source of autofluorescence is from yolk granules and the vitelline membrane [16] as shown in Fig. 2(c). Although the yolk does not contain any RFP or GFP, autofluorescence arises from endogenous fluorophores with emission spectra similar to that of NADH [17]. At 800 nm excitation wavelength, the fluorescence from the yolk is even brighter than the RFP. Because autofluorescence is a natural emission from the biological structures, it exists even before the first mitosis cycle. This special feature makes it particularly suitable as a guide star for imaging the embryo at the early stages. Figure 2(d) shows the wavefront measurement at a depth of 51 μm using autofluorescence for the guide star. During wavefront measurement, the laser is parked on the fluorophores indicated by the arrow. The laser power at the sample is 30 mw. The exposure time for a single measurement is 30 ms, which is over 25 times faster than the previous work using a nonlinear guide star [10]. The RMS error of the wavefront is 0.387 μm.

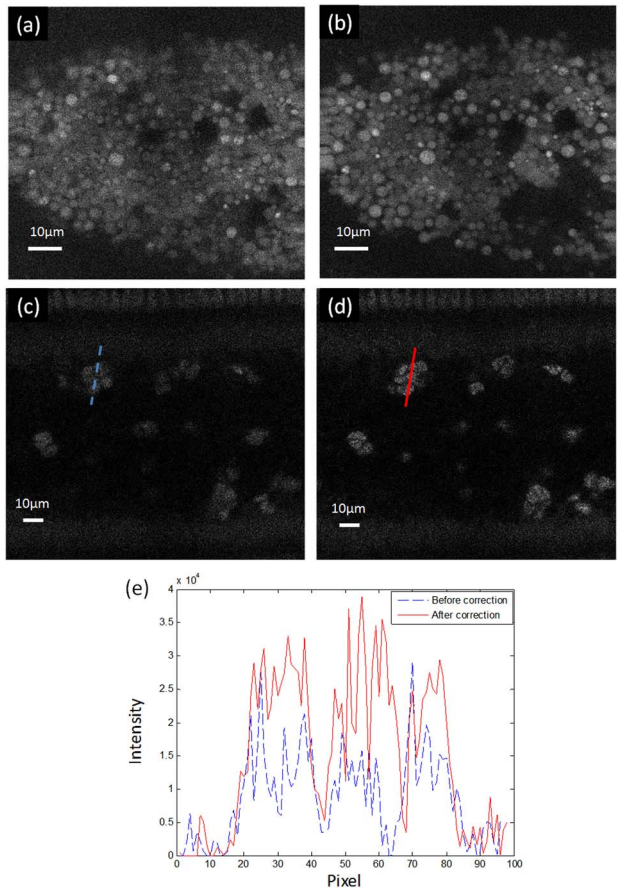

Fig. 3. Two-photon imaging of a live Drosophila embryo at a depth of 51 μm. The images of yolk autofluorescence before (a) and after correction. The RFP labeled nuclei structure before (a) and after (b) correction. The intensity profiles (e) along lines in (c) and (d) before (blue) and after (red) correction. The scale bars are 10 μm.

The two-photon images of yolk autofluorescence at a depth of 51 μm before and after correction are shown in Figs. 3(a) and 3(b). Each image is the maximum intensity projection of the three consecutive focal planes (1 plane/um), which takes 6 s to achieve the whole stacks. Because of the fast motion of the yolk during this imaging time, there is a small variation in structures shown in these two images. The excitation wavelength is set at 800 nm for maximizing the yolk autofluorescence. The structures of the endogenous fluorophores in the yolk are much clearer after correction, and the noise is reduced dramatically. A two-photon image of the RFP-labeled nuclei structure without correction is shown in Fig. 3(c). Compared with the yolk autofluorescence, less RFP can be selected for use as a guide star, and the intensity of the fluorescence is much lower. Figure 3(d) shows the two photon image after correction. The image after correction is much brighter than before correction. The intensity profile along the dashed lines across nuclei is shown in Fig. 3(e). The peak intensity increased by 2×. The fast direct wavefront measurement is particularly suitable to correct dynamic aberrations induced by live specimens. To validate this advantage, time-lapse wavefront aberrations were measured at a depth of 50 μm with a time resolution of 10 s (Media 1). Figure 4 shows the RMS wavefront change by around 0.1λ in the first 10 s. The fast wavefront measurement will benefit the correction of these dynamic aberrations.

We demonstrate an AO two-photon microscope using direct wavefront sensing. By using the autofluorescence from endogenous fluorophores as reference guide stars, the aberration in the middle of the embryo is able to be measured for the first time using a direct wavefront-sensing method. As a noninvasive method, the autofluorescent guide-star allows fast wavefront measurements in the middle of an embryo at the early dynamic stages. The

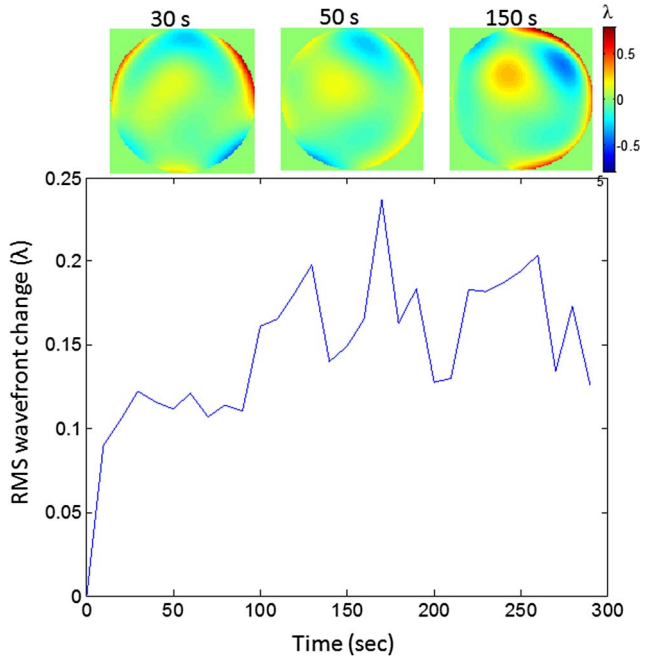

Fig. 4. RMS wavefront change during 300 s with a time resolution of 10 s (Media 1). The phase maps of the wavefront change at 30, 50, and 150 s are shown at the top.

experimental results show its potential to image the early mitosis process of the Drosophlia embryo *in vivo*. Using intrinsic fluorophores as guide stars will benefit a wide range of label-free nonlinear microscopes, such as second-harmonic generation, third-harmonic generation, and coherent anti-Stokes Raman scattering microscopes, which will be investigated in our future research.

The results presented herein were obtained at the W. M. Keck Center for Adaptive Optical Microscopy (CfAOM) at the University of California Santa Cruz. The CfAOM was made possible by the generous financial support of the W. M. Keck Foundation. We would like to thank Prof. William Sullivan, Dr. Shaila Kotadia, and Dr. Frederic Landmann of MCD Biology, UC Santa Cruz, for the Drosophila embryo samples and useful conversations. We also acknowledge the technical support from Ben Abrams in the UCSC Life Sciences Microscopy Center.

References

1. F. Helmchen and W. Denk, Nat. Methods **2**, 932 (2005).
2. J. A. Kubby, *Adaptive Optics for Biological Imaging* (CRC Press, 2013).
3. D. Debarre, E. J. Botcherby, T. Watanabe, S. Srinivas, M. J. Booth, and T. Wilson, Opt. Lett. **34**, 2495 (2009).
4. P. Marsh, D. Burns, and J. Girkin, Opt. Express **11**, 1123 (2003).
5. O. Albert, L. Sherman, G. Mourou, T. B. Norris, and G. Vdovin, Opt. Lett. **25**, 52 (2000).
6. N. Ji, D. E. Milkie, and E. Betzig, Nat. Methods **7**, 141 (2009).
7. X. Tao, O. Azucena, M. Fu, Y. Zuo, D. C. Chen, and J. Kubby, Opt. Lett. **36**, 3389 (2011).
8. X. Tao, B. Fernandez, O. Azucena, M. Fu, D. Garcia, Y. Zuo, D. C. Chen, and J. Kubby, Opt. Lett. **36**, 1062 (2011).
9. O. Azucena, J. Crest, S. Kotadia, W. Sullivan, X. Tao, M. Reinig, D. Gavel, S. Olivier, and J. Kubby, Opt. Lett. **36**, 825 (2011).
10. R. Aviles-Espinosa, J. Andilla, R. Porcar-Guezenec, O. E. Olarte, M. Nieto, X. Levecq, D. Artigas, and P. Loza-Alvarez, Biomed. Opt. Express **2**, 3135 (2011).
11. L. D. S. Haro and J. C. Dainty, Opt. Lett. **24**, 61 (1999).
12. W. R. Zipfel, R. M. Williams, R. Christie, A. Y. Nikitin, B. T. Hyman, and W. W. Webb, Proc. Natl. Acad. Sci. USA **100**, 7075 (2003).
13. K. M. Morzinski, K. B. W. Harpsee, D. T. Gavel, and S. M. Ammons, Proc. SPIE **6467**, 64670G (2007).
14. X. Tao, J. Crest, S. Kotadia, O. Azucena, D. C. Chen, W. Sullivan, and J. Kubby, Opt. Express **20**, 15969 (2012).
15. M. Ashburner, K. G. Golic, and R. S. Hawley, *Drosophila: A Laboratory Handbook*, 2nd ed. (Cold Spring Harbor Laboratory, 2004).
16. M. Mavrakis, R. Rikhy, M. Lilly, and J. Lippincott-Schwartz, Curr. Protoc. Cell Biol. **4**, 18 (2008).
17. J. P. Ogilvie, D. Debarre, X. Solinas, J. Martin, E. Beaurepaire, and M. Joffre, Opt. Express **14**, 759 (2006).